Inorganic Chemistry

Article

Cite This: Inorg. Chem. 2017, 56, 11862-11875

pubs.acs.org/IC

Understanding the Coordination Modes of [Cu(acac)$_2$(imidazole)$_{n=1,2}$] Adducts by EPR, ENDOR, HYSCORE, and DFT Analysis

Nadine Ritterskamp,[†] Katherine Sharples,[†] Emma Richards,*[,†] Andrea Folli,*[,†] Mario Chiesa,[‡] James A. Platts,[†] and Damien M. Murphy*[,†]

[†]School of Chemistry, Cardiff University, Park Place, Cardiff CF10 3AT, U.K.

[‡]Dipartimento di Chimica, Università di Torino, Via P. Giuria 7, 10125 Torino, Italy

Supporting Information

ABSTRACT: The interaction of imidazole with a [Cu(acac)$_2$] complex was studied using electron paramagnetic resonance (EPR), electron nuclear double resonance (ENDOR), hyperfine sublevel correlation spectroscopy (HYSCORE), and density functional theory (DFT). At low Im ratios (Cu:Im 1:10), a 5-coordinate [Cu(acac)$_2$Im$_{n=1}$] monoadduct is formed in frozen solution with the spin Hamiltonian parameters g_1 = 2.063, g_2 = 2.063, g_3 = 2.307, A_1 = 26, A_2 = 15, and A_3 = 472 MHz with Im coordinating along the axial direction. At higher Im concentrations (Cu:Im 1:50), a 6-coordinate [Cu(acac)$_2$Im$_{n=2}$] bis-adduct is formed with the spin Hamiltonian parameters g_1 = 2.059, g_2 = 2.059, g_3 = 2.288, A_1 = 30, A_2 = 30, and A_3 = 498 MHz with a poorly resolved ^{14}N superhyperfine pattern. The isotropic EPR spectra revealed a distribution of species ([Cu(acac)$_2$], [Cu(acac)$_2$Im$_{n=1}$], and [Cu(acac)$_2$Im$_{n=2}$]) at Cu:Im ratios of 1:0, 1:10, and 1:50. The superhyperfine pattern originates from two strongly coordinating N^3 imino nitrogens of the Im ring. Angular selective ^{14}N ENDOR analysis revealed the ^{N}A tensor of [34.8, 43.5, 34.0] MHz, with e^2qQ/h = 2.2 MHz and η = 0.2 for N^3. The hyperfine and quadrupole values for the remote N^1 amine nitrogens (from HYSCORE) were found to be [1.5, 1.4, 2.5] MHz with e^2qQ/h = 1.4 MHz and η = 0.9. ^{1}H ENDOR also revealed three sets of ^{H}A tensors corresponding to the nearly equivalent H^2/H^4 protons in addition to the H^5 and H^1 protons of the Im ring. The spin Hamiltonian parameters for the geometry optimized structures of [Cu(acac)$_2$Im$_{n=2}$], including *cis*-mixed plane, *trans*-axial, and *trans*-equatorial, were calculated. The best agreement between theory and experiment indicated the preferred coordination is *trans*-equatorial [Cu(acac)$_2$Im$_{n=2}$]. A number of other Im derivatives were also investigated. 4(5)-methyl-imidazole forms a [Cu(acac)$_2$(Im-**3**)$_{n=2}$] *trans*-equatorial adduct, whereas the bulkier 2-methyl-imidazole (Im-**2**) and benzimidazole (Im-**4**) form the [Cu(acac)$_2$(Im-**2,4**)$_{n=1}$] monoadduct only. Our data therefore show that subtle changes in the substrate structure lead to controllable changes in coordination behavior, which could in turn lead to rational design of complexes for use in catalysis, imaging, and medicine.

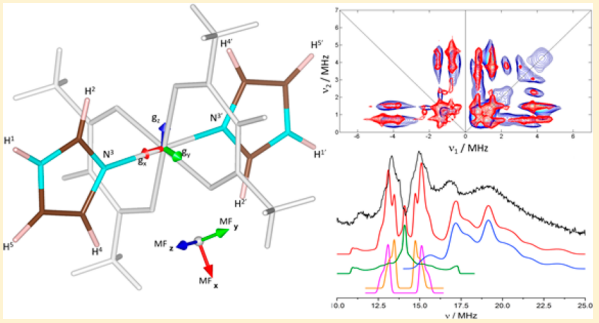

INTRODUCTION

The interaction of metal ions with bioligands, including proteins, nucleic acids, and their components, forms a central part of medicinal inorganic chemistry.[1,2] These interactions are important from a biological perspective because metals ions play an essential role in many biological processes.[3] Indeed, transition-metal ions and their complexes have become an important area of investigation as potentially new classes of anticancer agents.[2,4] However, problems often arise from the severe toxicity and inherent or acquired resistance to treatment using metal-based drugs. In many cases, a wide variety of metal complexes have been proposed as potential DNA intercalators[5] and, while new metal complexes based on Ru, As, Au, V, and Ti have all shown promise,[6] none are currently in clinical use.

By comparison, Cu has several characteristics that offer potential advantages in this role, including redox activity and endogenous presence within the human body.[4] The range of oxidation states, coordination geometries, and ligand structures available to Cu complexes allow for greater flexibility in design.[4] Unlike cisplatin and its derivatives, Cu complexes are believed to noncovalently bind to DNA either through major/minor grooves or via intercalation between base pairs, although other targets such as topoisomerase enzymes have also been proposed.

In these medicinal inorganic chemistry studies, in vivo activity is the ultimate test of the utility of such complexes. However, detailed structural information on how these metal complexes bind to receptors, base pairs, and indeed their mode of action is vital to obtain a complete understanding of the activity and hence enable a program of rational drug design. Many analytical techniques are therefore commonly used to analyze metal interactions and binding, including NMR, UV–vis, circular dichroism, isothermal calorimetry, and X-ray

Received: July 22, 2017
Published: September 21, 2017

DOI: 10.1021/acs.inorgchem.7b01874
Inorg. Chem. 2017, 56, 11862–11875

Scheme 1. Structures of (1) Imidazole (Im), (2) 2-Methyl-imidazole (Im-2), (3) 4(5)-Methyl-imidazole (Im-3) Showing the Resonance Structure, (4) Benzimidazole (Im-4), (5) Histidine, (6) Guanine, and (7) Adenine

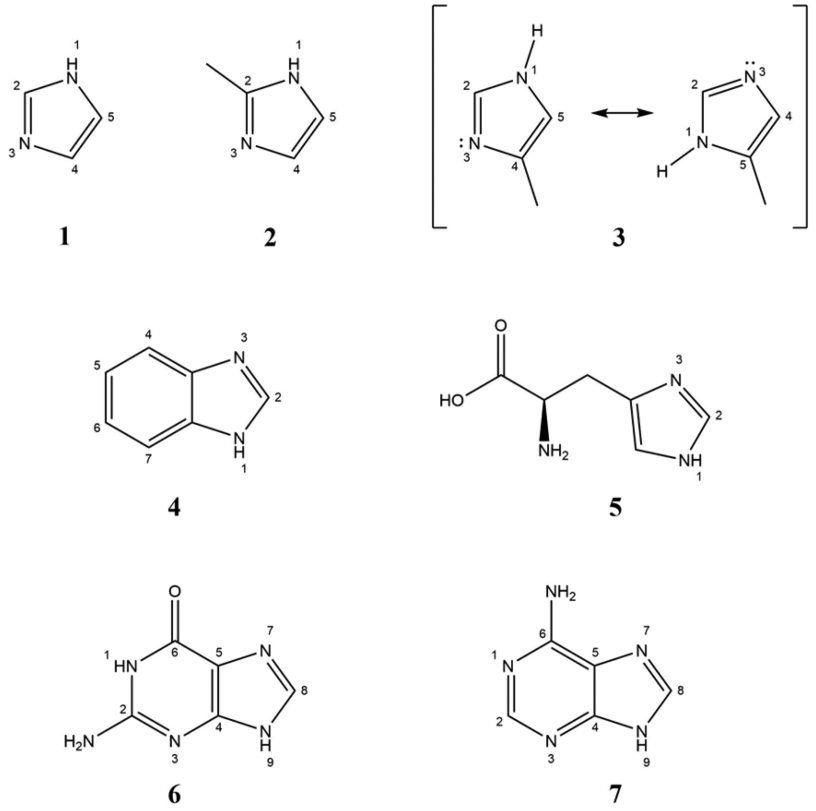

crystallography. For paramagnetic compounds, the resolution offered by NMR is often compromised and certainly considerably diminished. In such cases, the sophistication of information extracted by NMR can be matched by using electron paramagnetic resonance (EPR) spectroscopy. EPR and its related hyperfine techniques, including electron nuclear double resonance (ENDOR) and hyperfine sublevel correlation spectroscopy (HYSCORE), are extremely suitable spectroscopic methods to investigate both the electronic and geometric structure of metal complexes[7] and more generally copper active sites in biology.[8,9] Developing a greater appreciation of how the electronic and structural properties of the transition-metal complex governs the chemical nature of its interaction with biologically relevant substrates such as DNA is fundamentally important.

In this study, we exemplify the detailed information offered by the EPR techniques when investigating the coordination modes of Cu complexes, using imidazole as the choice substrate. Imidazole is common to both proteins and nucleic acids, as it is present in histidine residues and purine bases, respectively, rendering it biologically relevant. Furthermore, imidazole coordination to Cu(II) ions is prevalent in biological systems; coordination of histidine through the imino nitrogen (labeled N^3) as opposed to the amino nitrogen (N^1) of the imidazole ring is common to all copper proteins, while direct coordination of Cu(II) ions to DNA has been established to occur predominantly via the N^7 nitrogen of guanine (Scheme 1). The cytotoxicity of Cu complexes bearing substituted imidazole such as methyl- and phenyl-benzimidazoles has been demonstrated,[8] while a detailed EPR and ENDOR study of imidazole coordination to a Ru(III) anticancer agent was also reported recently.[9] Therefore, interactions between Cu(II) complexes and imidazole substrates are potentially important as model systems to better understand the nature of the Cu coordination mode with proteins and nucleic acids. Herein, we demonstrate how the coordination mode and structure of the resulting adducts can be investigated using a combination of advanced EPR techniques and density functional theory (DFT).

EXPERIMENTAL SECTION

Materials. The bis(acetylacetonato)-copper(II) complex (hereafter labeled [Cu(acac)$_2$]), imidazole (**1**) (hereafter labeled Im), 2-methyl-imidazole (Im-**2**), 4(5)-methyl-imidazole (Im-**3**), benzimidazole (Im-**4**), and fully deuterated imidazole-d$_4$ were all purchased from Sigma-Aldrich and used without further purification. Reagent grade (amylene stabilized) $CHCl_3$ was purchased from Fisher Scientific and dried over calcium hydride. Reagent grade DMF was sourced from Sigma-Aldrich and used as received. Deuterated solvents, including $CDCl_3$ and DMF-d_7, were obtained from Goss Scientific in sealed ampules and used without further purification.

Sample Preparation. A series of solutions containing [Cu(acac)$_2$] and imidazole in different ratios were prepared such that the ratio of copper to Im was systematically varied (0.5, 1, 2, 5, 10, 30, 40, and 50 equiv) while the concentration of [Cu(acac)$_2$] (0.02 M) and the composition of the $CHCl_3$:DMF (1:1) solvent was kept constant. The variable ratio study was monitored by CW X-band EPR in both frozen solution (140 K) and fluid solution (298 K). X-/Q-band EPR, ENDOR, and X-band HYSCORE studies were conducted on samples containing [Cu(acac)$_2$]:Im molar ratios of 1:0 and 1:50 at 10 K using 0.03 M solutions prepared in $CDCl_3$:DMF-d_7 (1:1). All samples for EPR, ENDOR, and HYSCORE measurements were prepared on the bench. Dry $CHCl_3$ and DMF solvents were used to prepare the solutions.

EPR/ENDOR Spectroscopy. The continuous wave (CW) X-band EPR measurements were performed on a Bruker EMX spectrometer

DOI: 10.1021/acs.inorgchem.7b01874
Inorg. Chem. 2017, 56, 11862−11875

utilizing an ER4119HS resonator, 100 kHz field modulation at 140 or 298 K, and typically using 10.17 mW MW power. The CW Q-band EPR and ENDOR measurements were recorded on a Bruker Elexsys E500 spectrometer using a Bruker ER5106 QT-E Q-band resonator operating at 10 kHz field modulation and 10 K for ENDOR (and at 100 kHz and 50 K for the EPR). The CW ENDOR spectra were obtained using 5 dB RF attenuation (80 W) from an ENI 3200L RF amplifier at 100 kHz RF modulation depth and 0.5 mW microwave power. Additional X-band Davies ENDOR measurements were also obtained. These Davies–ENDOR experiments[10] were recorded on a Bruker Elexsys E580 spectrometer and carried out using the following pulse sequence: π-T-$\pi/2$-τ-π-τ-echo. The experiments were done with mw pulse lengths of t_π = 256 ns, $t_{\pi/2}$ = 128 ns, and an interpulse time τ of 800 ns. An rf τ pulse of variable frequency and a length of 18 μs were applied during time T of 20 μs.

Hyperfine Sublevel Correlation (HYSCORE) Experiments. The HYSCORE experiments[11] were performed on a Bruker Elexsys E580 spectrometer utilizing a Bruker EN 4118X-MD4 pulsed EPR/ENDOR resonator and 10 K. The experiments were carried out with the pulse sequence $\pi/2$-τ–$\pi/2$-t_1-π-t_2-$\pi/2$-τ-echo. The microwave pulse lengths $t_{\pi/2}$ = 16 ns and t_π = 16 ns were adopted. The time intervals t_1 and t_1 were varied in steps of 16 ns starting from 100 to 3300 ns. The fixed interpulse delay (τ) values are specified in the figure captions. The adopted shot repetition rate was 1 kHz. A four-step phase cycle was used for eliminating unwanted echoes. Spectra were recorded at two magnetic field positions corresponding to B_0 = 338.6 mT ($g_\perp$) and B_0 = 283.2 mT (corresponding to the single crystal-like position, m_I = −3/2, where only molecules with their g_z axis aligned along the external magnetic field are selected). The magnetic field was measured by means of a Bruker ER035 M NMR gauss meter.

All of the EPR, ENDOR, and HYSCORE simulations were performed using the Easyspin[12] software package running within the MathWorks MatLab environment. The rotational correlation times for the different complexes were computed in Easyspin assuming an isotropic rotational diffusion in the fast motion regime. Once a value of the correlation time is imposed, line widths are computed using the Kivelson formulas[13] within the Redfield limit (motional narrowing).[14]

DFT Calculations. Geometries of all species were fully optimized without symmetry constraint using the M06-2X[15] meta-hybrid functional and a basis set of 6-31+G(d,p)[16−18] on light atoms and Stuttgart–Dresden effective core potential and basis set on Cu[19] using the Gaussian09 suite.[20] The resulting geometries were used to estimate EPR parameters in ORCA[21] using the hybrid PBE0[22] functional and basis set of EPRII[23] for light atoms and the Core Properties all-electron basis set for Cu[24] with spin–orbit effects accounted for in a mean field approach.[25]

RESULTS AND DISCUSSION

CW EPR. The experimental and simulated CW EPR spectrum of the unbound $[Cu(acac)_2]$ complex in $CHCl_3$:DMF is shown in Figure 1a (and also in the Supporting Information, Figure S1a). Although $[Cu(acac)_2]$ is readily soluble in most organic solvents, the Im substrate is not. Hence, for all EPR measurements, the $[Cu(acac)_2]$ complex bearing increasing concentrations of Im was dissolved in a $CHCl_3$:DMF (1:1) solvent system to ensure complete solubility of Im. The resulting spin Hamiltonian parameters for the unbound $[Cu(acac)_2]$ complex in this $CHCl_3$:DMF solvent system are listed in Table 1. As discussed previously by us,[26] the g and ^{Cu}A parameters observed for unbound $[Cu(acac)_2]$ in frozen solutions depend subtly on the choice of solvent used, and in most cases will produce a well-defined signal with the ^{63,65}Cu isotope splitting clearly evident on the low field hyperfine component. While very dry noncoordinating solvents such as $CHCl_3$:Tol give values of g_{iso} = 2.117 and a_{iso} = 237 MHz, weakly coordinating solvents such as $CHCl_3$:DMF (and even slightly wet $CHCl_3$:Tol solvents)[26] produce notably different

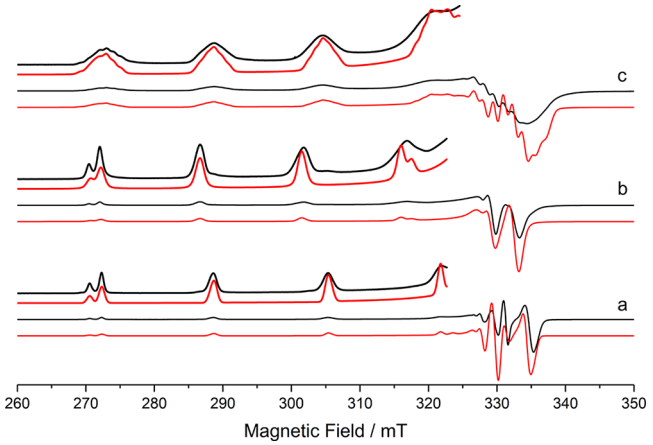

Figure 1. Experimental (black) and simulated (red) CW X-band EPR spectra of (a) unbound $[Cu(acac)_2]$, (b) the $[Cu(acac)_2Im]$ monoadduct (Cu:Im ratio of 1:5), and (c) the $[Cu(acac)_2Im_2]$ bis-adduct (Cu:Im ratio of 1:50). The spectra were recorded at 140 K in a $CHCl_3$:DMF (1:1) solvent. The simulation parameters are listed in Table 1.

values, as observed in the current case with g_{iso} = 2.135 and a_{iso} = 196 MHz.

To investigate the nature and coordination mode of the adducts formed between $[Cu(acac)_2]$ and Im, a speciation study was first performed by increasing the Cu:Im ratios from 1:0 to 1:50 in the $CHCl_3$:DMF (1:1) solvent. The complete set of resulting CW EPR spectra for all ratios investigated are shown in the Supporting Information (Figures S1a–i). At 1 equiv of Cu:Im, a mixed EPR spectrum is observed, composed of unbound $[Cu(acac)_2]$ bearing no Im coordination along with a second signal readily assigned to a bound $[Cu(acac)_2Im]$ monoadduct (see Supporting Information, Figure S1b). At 1:5 equiv of Cu:Im, only this $[Cu(acac)_2Im]$ monoadduct is detected in the EPR spectrum (Supporting Information, Figure S1d). As the Cu:Im ratio is increased further, a third signal appears in the spectrum which can be readily assigned to a $[Cu(acac)_2Im_2]$ bis-adduct (vide infra). At 1:50 equiv of Cu:Im, only this $[Cu(acac)_2Im_2]$ bis-adduct is observed in the spectrum (Supporting Information, Figure S1i).

The experimental and simulated EPR spectra of the $[Cu(acac)_2Im_{n=1,2}]$ mono- or bis-adducts (obtained at Cu:Im ratios of 1:5 and 1:50) are shown in Figures 1b and c, respectively. The resulting spin Hamiltonian parameters are listed in Table 1. The $[Cu(acac)_2Im]$ monoadduct reveals a small increase in the g_3 value (Δg_z = 0.022) and a concomitant decrease in A_3 (ΔA_z = 48 MHz) relative to the unbound $[Cu(acac)_2]$ complex in the weakly coordinating $CHCl_3$:DMF (1:1) solvent system. These shifts in g_3/A_3 are even larger when using dry noncoordinating $CHCl_3$:Tol (1:1) solvent (cf. Δg_z = 0.055 and ΔA_z = 100 MHz;[26] see Table 1) and are indicative of axial substrate coordination to the predominantly square planar $Cu-O_4$ environment in $[Cu(acac)_2]$.[27] The latter deviations observed for Im coordination (relative to the values for $[Cu(acac)_2]$ in dry noncoordinating $CHCl_3$:Tol) are notably larger compared to those reported for various substituted pyridines (cf. Δg_z = 0.043, ΔA_z = 74 MHz),[27] indicating a stronger axial coordination of Im with the $[Cu(acac)_2]$ complex. Because Im is a stronger base compared to pyridine, this stronger interaction is expected. It should also be briefly mentioned that the axially coordinated $[Cu(acac)_2Py]$ mono-adducts (where Py refers to pyridine, methyl-pyridine, or

DOI: 10.1021/acs.inorgchem.7b01874
Inorg. Chem. 2017, 56, 11862–11875

Table 1. Spin Hamiltonian g and ^{Cu}A Parameters of $[Cu(acac)_2Im_{n=0,1,2}]$ Complexes with Comparative Literature Values of *cis*-Equatorial and *trans*-Equatorial $Cu-O_4N_2$ Complexes[a]

	g_1	g_2	g_3	g_{iso}	$^{Cu}A_1$	$^{Cu}A_2$	$^{Cu}A_3$	a_{iso}	ref
				unbound					
$[Cu(acac)_2]$[f]	2.060[b]	2.060[b]	2.285[b]	2.135	−35[c]	−35[c]	−520[d]	−196[e]	tw
$[Cu(acac)_2]$[g]	2.048	2.052	2.252	2.117	−81	−58.5	572	−237	26
DFT	2.053	2.056	2.188	2.099	−130	−134	−891	−385	tw
				monoadduct					
$[Cu(acac)_2Im]$[f]	2.063[b]	2.063[b]	2.307[b]	2.114	26[c]	15[c]	472[d]	171[e]	tw
$[Cu(acac)_2Im]$[h]	2.060	2.060	2.260	2.127			557		31
$[Cu(acac)_2$(Im-**2**)$]$	2.064	2.064	2.307	2.145	26[c]	15[c]	469[d]	170[e]	tw
$[Cu(acac)_2$(Im-**3**)$]$	2.064	2.064	2.307	2.145	26[c]	15[c]	472[d]	171[e]	tw
$[Cu(acac)_2$(Im-**4**)$]$	2.063	2.063	2.305	2.144	26[c]	15[c]	475[d]	172[e]	tw
DFT	2.063	2.076	2.221	2.120	−34	−96	−855	−329	tw
				bis-adduct					
$[Cu(acac)_2Im_2]$[f]	2.059[b]	2.059[b]	2.288[b]	2.135	30[c]	30[c]	498[d]	186[e]	tw
$[Cu(acac)_2$(Im-**3**$)_2]$[f]	2.063	2.063	2.289	2.138	30[c]	30[c]	496[d]	185[e]	tw
				reference complexes					
	g_1	g_2	g_3	g_{iso}	$^{Cu}A_1$	$^{Cu}A_2$	$^{Cu}A_3$	a_{iso}	ref
				cis-equatorial					
$[Cu(acac)_2en]$[i]	2.033	2.033	2.184	2.083	77	77	621		32
$[Cu(hfacac)_2bipy]$[j]	2.056	2.056	2.299	2.137	77	77	486	213	33
$[Cu(nap)_2bipy]$[k]	2.066	2.066	2.281	2.137			502		34
				trans-equatorial					
$[Cu(acac)_2Im_2]$[h]	2.047	2.047	2.260	2.118			547		31
$[Cu(AcO)_2Im_2]$[l]			2.267				486		35
$[Cu(nap)_2(4\text{-picoline})_2]$[k]	2.066	2.066	2.304	2.145			486		29
$DFT_{cis\text{-mixed plane}}$	2.070	2.109	2.248	2.142	47	−76	−834	−288	tw
$DFT_{trans\text{-axial}}$	2.080	2.083	2.245	2.136	−21	−30	−843	−298	tw
$DFT_{trans\text{-equatorial}}$	2.060	2.110	2.243	2.138	−151	154	−794	−264	tw

[a]tw = this work; $^{Cu/N}A$ values given in units of MHz. [b]±0.003. [c]±5. [d]±3. [e]±2. [f]$CHCl_3$:DMF (1:1). [g]$CHCl_3$:Tol (1:1). [h]DMSO:H_2O (90:10). [i]Single crystal. [j]Doped solid of $[Zn(hfacac)_2Bipy]$:$[Cu(hfacac)_2Bipy]$ (50:1). [k]$CHCl_3$:CH_2Cl_2 (1:1). [l]H_2O. Ligand abbreviations: hfacac = hexafluoroacetylacetonate and nap = 2-nitroacetophenone.

Scheme 2. Schematic Illustration Showing (a) Unbound $[Cu(acac)_2)]$ and (b) $[Cu(acac)_2Im]$ Monoaxial Adduct and the Structural Isomers of the $[Cu(acac)_2Im_2]$ Bis-Adducts, Including (c) *trans*-Axial, (d) *cis*-Mixed Plane, (e) *trans*-Equatorial, and (f) *cis*-Equatorial

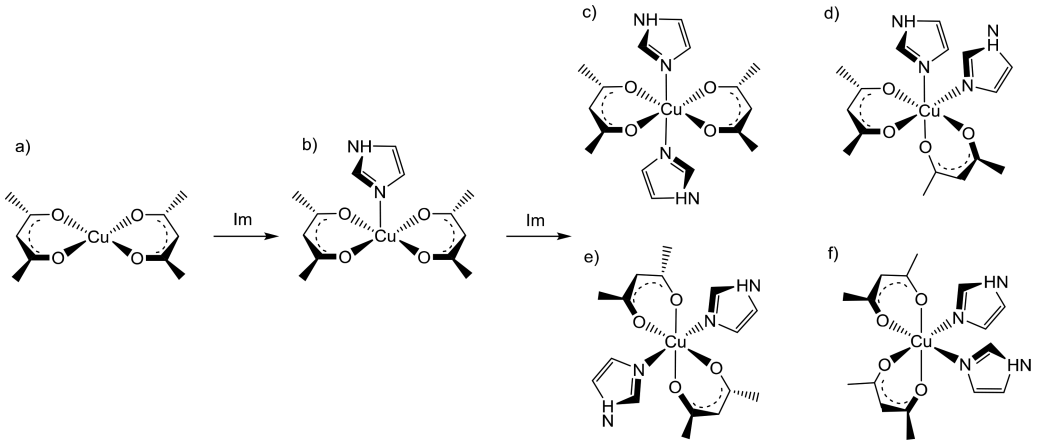

amino-methyl substituted pyridines) readily form at Cu:Py ratios of 1:1 in dry noncoordinating $CHCl_3$:Tol solvents.[27] Even at Cu:Py ratios of 1:50, only $[Cu(acac)_2Py]$ monoadducts were formed. In the current work, the weakly coordinating $CHCl_3$:DMF solvent system contributes to the higher Cu:Im ratios of 1:5 required to form the axial $[Cu(acac)_2Im]$ monoadduct. As expected, the ^{14}N superhyperfine interaction in these axially coordinated square planar monoadduct complexes bearing nitrogen-bases (such as $[Cu(acac)_2Im]$) is not visible in the EPR spectrum[28] owing to the predominantly d_{xy} ground state for the copper(II) ion.

At higher Cu:Im ratios (1:50), a second copper(II) signal is clearly visible in the EPR spectrum (Figure 1c and Supporting Information, Figures S1g–i). This appears at the expense of the $[Cu(acac)_2Im]$ monoadduct signal. The predominantly axial EPR signal (Table 1) of this new adduct is characterized by a

DOI: 10.1021/acs.inorgchem.7b01874
Inorg. Chem. 2017, 56, 11862–11875

pronounced ^{14}N superhyperfine splitting, which is evident in the parallel and perpendicular ^{Cu}A hyperfine components. Analysis of the ^{14}N superhyperfine pattern appears to indicate the presence of two equivalent nitrogen nuclei (I = 1) originating from two (equatorially) bound Im bases, presumably from a six-coordinate $[Cu(acac)_2Im_2]$ bis-adduct. The equatorial coordination of the Im appears most likely, as opposed to the bis-axial coordination, owing to the large superhyperfine splitting, as widely reported in the literature for equatorially bound nitrogen bases.[29,30] The spin Hamiltonian g and ^{Cu}A parameters for this $[Cu(acac)_2Im_2]$ bis-adduct are listed in Table 1. The large ^{14}N hyperfine values used in the EPR simulation were extracted from the ENDOR spectra (vide infra) and are given later in Table 4.

The structural nature of the $[Cu(acac)_2Im_2]$ bis-adduct cannot be reliably extracted from the frozen solution EPR spectrum alone. The observed g values ($g_\perp$ = 2.059 and $g_\parallel$ = 2.288) are consistent with a Cu(II) center in an axially elongated tetragonal ligand field ($g_\parallel > g_\perp$) environment.[29,34] The ^{14}N superhyperfine pattern indicates that both Im substrates must coordinate in the equatorial (xy) plane, limiting the plausible coordination geometries to *trans*-equatorial or *cis*-equatorial (Scheme 2). Representative g and ^{Cu}A parameters for copper(II) complexes possessing a $Cu-O_4N_2$ environment with *cis*-equatorial and *trans*-equatorial geometries (with respect to the nitrogen ligands) are listed in Table 1. As can be seen from the Table, there is a reasonable variation in the g and ^{Cu}A values for both coordination isomers, suggesting that the *cis*- and *trans*-equatorial conformations of $[Cu(acac)_2Im_2]$ cannot be easily differentiated by EPR alone. While the point group symmetries of MA_4B_2-type complexes should in principle be different for *cis*- versus *trans*-isomers producing axial or rhombic $\boldsymbol{g}$ tensors, the distortion that occurs in the complexes coupled with the broad line-widths in frozen solution will mean that any difference in g and ^{Cu}A anisotropy will not be visible at X- or Q-band frequencies. It should also be mentioned that, despite the strength of the base, Im itself does not displace the acac ligand in the complex because the spectral features observed in Figure 1b are not consistent with those arising from $[Cu(Im)_4]$.[36,37]

Formation of the mono- and bis-adducts are also expected to be temperature dependent. At 140 K, the X-band EPR spectra showed a distribution of copper species, including those arising from unbound $[Cu(acac)_2]$, $[Cu(acac)_2Im]$, and $[Cu(acac)_2Im_2]$, depending on the ratio of Cu to Im used (Supporting Information, Figure S1). At a Cu:Im ratio of 1:10, the 140 K spectrum was almost exclusively composed of $[Cu(acac)_2Im]$ adducts (Figure 1b), whereas at a Cu:Im ratio of 1:50, the spectrum was dominated by $[Cu(acac)_2Im_2]$ (Figure 1c). However, a wider distribution of copper adducts was observed in the X-band EPR spectra recorded at 298 K, depending on the Cu:Im ratios used (Figure 2). Using the anisotropic spin Hamiltonian parameters listed in Table 1, the isotropic EPR spectra were simulated in the fast motional regime, and the resulting rotational correlational times (τ_R) were obtained by simulation (using Easyspin[12−14]) (Table 2). Representative examples of the simulated isotropic EPR spectra for the Cu:Im ratios of 1:0 and 1:50 are shown in Figure 3 (the corresponding simulation for the Cu:Im ratio of 1:10 is given in the Supporting Information, Figure S2). According to the analysis of the isotropic simulations, the EPR spectrum recorded using a Cu:Im ratio of 1:10 contains a contribution from both unbound $[Cu(acac)_2]$ (45.5%) and $[Cu(acac)_2Im]$ (54.5%). However, for a Cu:Im ratio of 1:50, the room

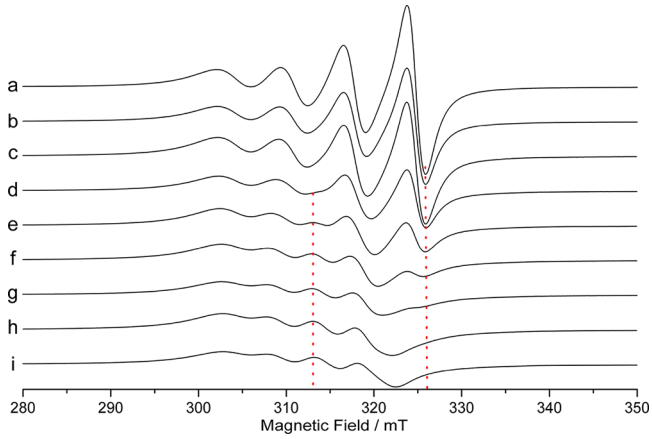

Figure 2. CW X-band EPR spectra (298 K) of $[Cu(acac)_2]$ recorded with increasing Cu:Im ratios of (a) 1:0, (b) 1:1, (c) 1:2, (d) 1:5, (e) 1:10, (f) 1:20, (g) 1:30, (h) 1:40, and (i) 1:50.

temperature spectrum (Figure 3) contains a contribution from both $[Cu(acac)_2Im]$ (79.0%) and $[Cu(acac)_2Im_2]$ (21.0%), unlike the 140 K equivalent spectrum (Figure 1c), which revealed only the presence of $[Cu(acac)_2Im_2]$ species. These results highlight the expected temperature dependency of Im binding.

It should also be noted that the integrated EPR signal intensity in the room temperature spectra was found to decrease by ca. 45% as the Im concentrations in solution increased (Figure 2). This observation was also detected in the 140 K frozen solution EPR spectra (Supporting Information, Figure S1). Anderson et al.[37] also reported a reduced Cu(II) EPR signal intensity in solutions of Cu(II) salts bearing high Im concentrations and ascribed the observation to the possible precipitation of coordination polymers such as $[Cu(Im)_2(Im^-)]_n^{m+}$, whereby anionic Im^- acted as a bridging ligand. Certainly, under basic conditions, deprotonation at the N^1 atom of imidazole produces an imidazolate anion (Im^-), which is well-documented to bridge transition-metal ions through N^1 and N^3 coordination.[38] In fact imidazolate bridges are evident in some multimetal enzymes, including SOD,[39] and can mediate magnetic couplings between the metal centers.[40] Therefore, although no precipitate was evident in the current study, it seems reasonable that the loss in Cu(II) signal intensity may at least in part be attributed to the spin−spin interactions occurring in Im^- bridged $[Cu(acac)_2(Im)(Im^-)]_n^{m+}$-type polymers, similar to those described by Anderson et al.[37]

DFT Analysis of the Adducts. The geometry optimized structure of the monoaxial adduct was calculated and found to be square pyramidal, bearing an axially coordinated Im ligand (Figure 4a) with a Cu−N distance of 2.27 Å and all Cu−O distances between 1.97 and 1.98 Å. The geometry optimized *cis*-mixed plane structure of the $[Cu(acac)_2Im_2]$ bis-adduct was characterized by one axial and one equatorial Im ligand (Figure 4b) at Cu−N distances of 2.35 and 2.08 Å, respectively. Cu−O distances were found to range between 1.99 and 2.01 Å (the three equatorial) and one axial at 2.22 Å (i.e., Jahn−Teller elongation of one Cu−N and one Cu−O bonds).

The *trans*-axial $[Cu(acac)_2Im_2]$ bis-adduct was found to have both of the Im ligands in axial positions with Cu−N distances of 2.35 and 2.34 Å. The Cu−O bond lengths range between 1.99 and 2.00 Å. In contrast, the *trans*-equatorial $[Cu(acac)_2Im_2]$ adduct was established to be a Jahn−Teller

DOI: 10.1021/acs.inorgchem.7b01874
Inorg. Chem. 2017, 56, 11862−11875

Table 2. Rotational Correlation Times and Line Width Contributions for the Room Temperature (298 K) X-Band CW EPR Spectra of the $[Cu(acac)_2Im_{n=0,1,2}]$ Complexes[a]

species	lw $m_I = +3/2$	lw $m_I = +1/2$	lw $m_I = -1/2$	lw $m_I = -3/2$	τ_R
$[Cu(acac)_2]$	151.33	92.48	44.84	11.21	50[b]
$[Cu(acac)_2Im]$	156.94	98.09	50.44	14.01	45[c]
$[Cu(acac)_2Im_2]$	137.32	84.07	42.04	11.21	40[b]

[a]The line widths (lw) of each of m_I line are given in MHz. The rotational correlation times (τ_R) are given in ps with uncertainties of [b]±10 ps. [c]±20 ps.

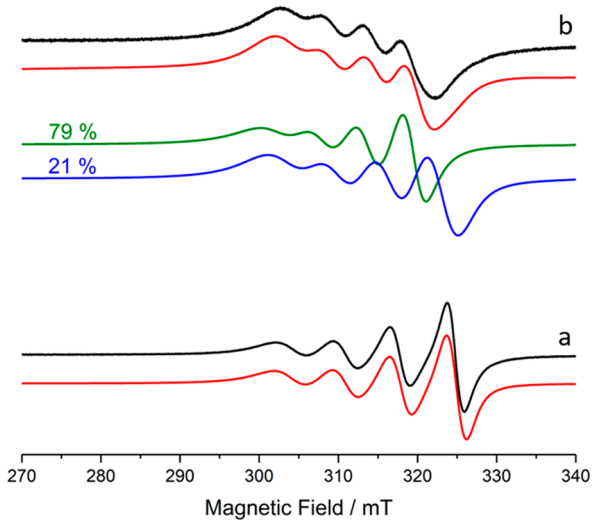

Figure 3. Experimental (black) and simulated (red) X-band CW EPR spectra (298 K) of $[Cu(acac)_2]$ recorded with a Cu:Im ratios of (a) 1:0 and (b) 1:50. The deconvoluted simulation of b, shown in the green and blue traces, is due to 79% $[Cu(acac)_2Im]$ (green) and 21% $[Cu(acac)_2Im_2]$ (blue). The spectra were recorded in a $CHCl_3$:DMF (1:1) solvent. The simulation parameters are listed in Table 2.

distorted octahedral complex with both Im ligands occupying equatorial positions (Figure 4d) at Cu−N distances equal to 2.00 Å. Two Cu−O distances measure 2.05 Å and correspond to the equatorial oxygen atoms, while the remaining two Cu−O bonds, measuring 2.17 Å, are consistent with the oxygen atoms in axial positions. It should be noted that the *trans*-equatorial structure was predicted to lie 23.0 kJ mol^{-1} higher in energy compared to the *trans*-axial structure and 17.3 kJ mol^{-1} higher than the *cis*-mixed plane at the M06-2X (PBE0) level, and we ascribe these energy differences to the choice of functional and basis set used (see Supporting Information).

^{1}H ENDOR. While EPR cannot reliably distinguish between the different structural isomers of the *cis*-mixed plane or *trans*-equatorial $[Cu(acac)_2Im_2]$ adducts, ^{1}H ENDOR experiments can aid the discrimination between possible structures formed in frozen solution. We previously showed how important structural information on the coordination geometry of $[Cu(acac)_2]$ adducts can be revealed through a complete angular selective ^{1}H ENDOR analysis, including the tilt angle and orientation of coordinated pyridine substrates with respect to the Cu−O4 plane of $[Cu(acac)_2]$.[27]

Therefore, the Q-band ^{1}H ENDOR spectra of the bis-adduct was recorded using both protic and deuterated Im (i.e., $[Cu(acac)_2Im_2]$ and $[Cu(acac)_2(Im\text{-}d_4)_2]$) using fully deuterated $CHCl_3$:DMF solvents (see Supporting Information, Figure S3). This experiment enabled the Im derived proton couplings to be readily identified in the spectra because the remaining signals in the ENDOR spectra must arise from the protons of the bis(acetylacetonate) ligand itself. The ^{1}H ENDOR spectra of this ligand in the unbound $[Cu(acac)_2]$ complex is deceptively complex, bearing couplings that arise from the methine protons, the fully averaged methyl group protons, and a subset of methyl group protons undergoing hindered rotation on the EPR time scale such that a very anisotropic hyperfine tensor is produced (as revealed by variable temperature X-band Mims ENDOR).[26] This hindered rotation was found to occur in 120° jumps such that a large $A_{dipolar}$ and a_{iso} component (greater than the fully averaged methyl group tensor) is always observed in the spectra.[26] In the current system, these bis(acetylacetonate) derived protons are still visible in the angular selective ^{1}H ENDOR spectra of $[Cu(acac)_2Im_2]$ bearing protic Im (Figure 5). However, for clarity, only the ^{1}H ENDOR signals originating from the coordinated Im substrates are shown in the simulation (Figure 5), and for this reason, not all of the experimental lines are reproduced by the simulation. The resulting experimentally derived principal hyperfine values for the Im protons are listed in Table 3.

A satisfactory fit to the experimental spectra was obtained using three sets of hyperfine tensors (labeled sets I, II, and III in Table 3). The deconvoluted simulation is shown in the Supporting Information (Figure S5). The DFT calculated hyperfine tensors were used as the starting point in the simulation, and the parameters adjusted and modified only slightly to obtain the best visual fit with the experimental spectra. Owing to the different proton environments in the bound Im substrates, the observation of these different tensors is not unexpected. The hyperfine values were compared to the theoretical ^{1}H hyperfine tensors calculated by DFT (Table 3). In all cases, the Im derived protons from the $[Cu(acac)_2Im_2]$ bis-adducts, including the *cis*-mixed plane, *trans*-axial, or *trans*-equatorial structures, produced different theoretical couplings. However, the hyperfine tensors predicted for the structures bearing one or two equatorially bound Im substrates (*i.e., cis*-mixed plane and *trans*-equatorial; Scheme 2 and Figures 4b and d) most closely matched the experimental values so that sets I, II, and III can be assigned to the H^2/H^4 protons, the H^5 protons, and the amine H^1 proton of the Im ligand, respectively.

The higher symmetry *trans*-equatorial structure, containing two equivalent Im substrates, would be expected to produce an ENDOR spectrum less complex compared to that of the *cis*-mixed plane structure where both Im substrates are inequivalent, leading to more hyperfine couplings. Therefore, although the angular selective ^{1}H ENDOR data appear to be more consistent with the *trans*-equatorial structure; nevertheless, we cannot confidently discriminate between the *cis*- and *trans*-structures (Figures 4b and d) based on ^{1}H ENDOR measurements alone. For this reason, ^{14}N ENDOR and HYSCORE were employed.

^{14}N ENDOR and HYSCORE. The nitrogen superhyperfine pattern observed in the CW X-band EPR spectrum (Figure 1c)

DOI: 10.1021/acs.inorgchem.7b01874
Inorg. Chem. 2017, 56, 11862−11875

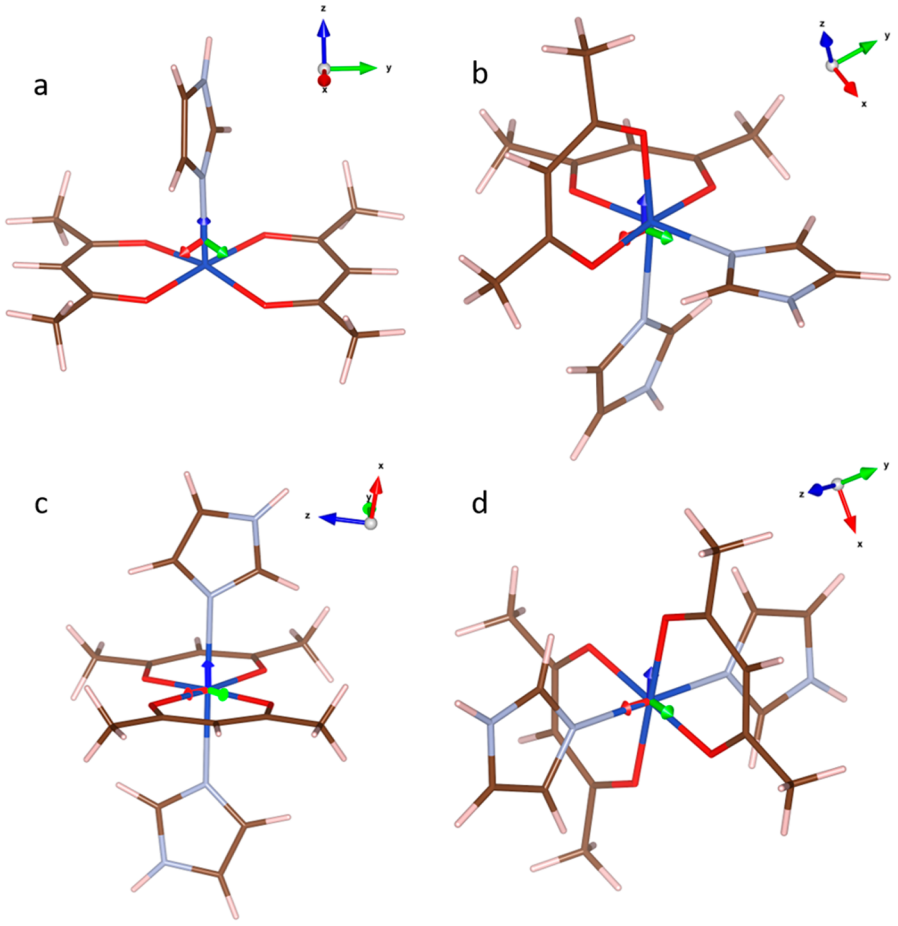

Figure 4. Geometry optimized structures for (a) monoaxial [$Cu(acac)_2Im$], (b) *cis*-mixed plane, (c) *trans*-axial, and (d) *trans*-equatorial isomers of the [$Cu(acac)_2Im_2$] adduct. In each structure, the *g*-frame is reported on the Cu atom with the same color coding as the molecular frame on the right-hand side of each structure: *x* (red), *y* (green), and *z* (blue).

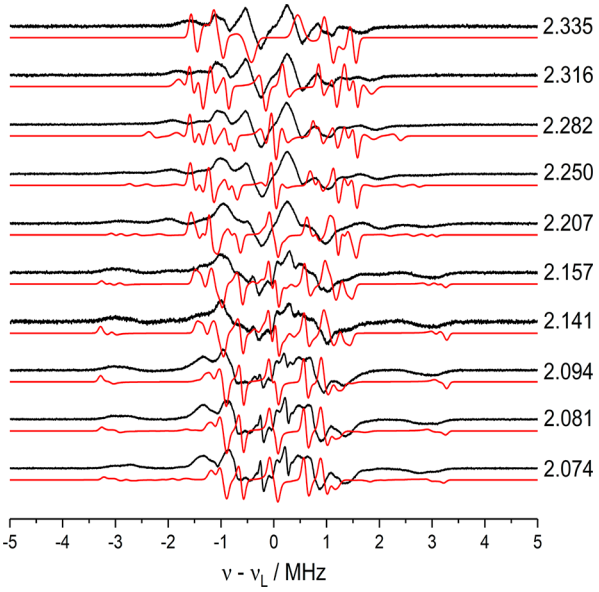

Figure 5. CW Q-band ^1H ENDOR spectra (10 K) of the [$Cu(acac)_2Im_2$] bis-adduct dissolved in dry $CDCl_3$:DMF-d_7 (1:1) recorded at the field positions corresponding to the *g*-values indicated beside each spectrum. The corresponding simulations are shown in red.

is potentially a rich source of structural information on the coordination mode of the [$Cu(acac)_2Im_2$] bis-adduct. However, line-broadening effects lead to poor resolution in the frozen solution spectra which prevents the accurate determination of the nitrogen hyperfine from the EPR spectrum alone. The ^{14}N hyperfine ($^N\boldsymbol{A}$) and quadrupole ($^N\boldsymbol{Q}$) tensors can in principle be determined by the hyperfine techniques such as ENDOR and HYSCORE. The strongly coupled ^{14}N observed in the EPR spectrum (N^3, Scheme 1) can be analyzed by ENDOR whereas the remote ^{14}N of the Im ring (N^1, Scheme 1) can be detected by HYSCORE. When combined, these methods can be utilized to further investigate the structure of the bis-adduct. Indeed, Iwaizumi et al.[35] demonstrated that ^{14}N ENDOR spectroscopy could be used to discriminate between copper complexes bearing pseudoplanar arrays of donor sets, including N4, *cis*-N2O2, and *trans*-N2O2. However, depending on the hybridized state of the nitrogens or the changes in symmetry of the complex, this simple correlation between ^{14}N hyperfine and structure may be of limited diagnostic value and must be treated cautiously.

The angular selective CW Q-band ^{14}N ENDOR spectra were therefore recorded, and the resulting experimental and simulated spectra are shown in Figure 6a. The spectra were successfully simulated using a single ^{14}N tensor, indicative of an equivalent nitrogen environment (with no evidence of a second strongly coupled nitrogen), and the resulting parameters are listed in Table 4. The hyperfine tensor was found to deviate

DOI: 10.1021/acs.inorgchem.7b01874
Inorg. Chem. 2017, 56, 11862−11875

Table 3. ^{1}H Principal Hyperfine Values for [Cu(acac)$_2$Im$_2$] Dissolved in CDCl$_3$:DMF-d_7 (1:1)

atom	α	β	γ	A_x	A_y	A_z	a_{iso}
			[Cu(acac)$_2$Im$_{n=2}$]: experimental (ENDOR)				
set I (H^2/H^4)	20[b]	45[b]	−10[b]	0.10[c]	−0.14[c]	6.55[c]	2.17
set II (H^5)	10[b]	75[b]	0[b]	1.21[c]	1.17[c]	2.43[c]	1.60
set III (H^1)	30[b]	20[b]	−30[b]	3.15[c]	1.80[c]	1.95[c]	2.30
			monoaxial [Cu(acac)$_2$Im$_{n=1}$]: DFT				
H^4	−19.9	70.3	22.8	2.83	−1.47	−1.39	−0.01
H^2	−30.3	40.90	−33.90	−2.06	−1.83	3.98	0.03
H^5	−2.0	83.50	37.10	0.76	−0.48	−0.47	−0.06
H^1	−26.9	21.7	−42.5	−0.56	−0.56	0.90	−0.07
			cis-mixed plane [Cu(acac)$_2$Im$_{n=2}$]: DFT				
H^4	−25.4	32.2	11.8	−1.61	−1.80	3.38	−0.01
H^2	−3.0	56.0	−0.10	3.25	−1.65	−1.55	0.02
H^5	5.1	14.4	41.00	−0.48	−0.48	0.8	−0.05
H^1	−6.8	74.7	−4.8	0.83	−0.55	−0.54	−0.09
H$^{4\prime}$	1.7	87.8	−44.0	−0.65	6.03	0.17	1.85
H$^{2\prime}$	−2.6	88.8	36.60	−1.22	5.95	−0.54	1.40
H$^{5\prime}$	38.1	0.8	−55.10	0.33	2.11	0.24	0.89
H$^{1\prime}$	−1.2	87.2	13.9	0.47	2.42	0.65	1.18
			trans-axial [Cu(acac)$_2$Im$_{n=2}$]: DFT				
H^4	13.6	64.1	19.4	2.76	−1.39	−1.47	−0.03
H^2	−21.2	38.8	44.8	−2.01	−1.79	3.83	0.01
H^5	3.8	84.4	34.8	0.74	−0.47	−0.47	−0.07
H^1	−10.5	19.4	39.9	−0.57	−0.56	0.86	−0.09
H$^{4\prime}$	−13.5	64.9	48.6	2.69	−1.35	−1.43	−0.03
H$^{2\prime}$	16.5	39.5	26.1	−2.07	−1.83	3.92	0.01
H$^{5\prime}$	−6.0	86.2	39.2	0.74	−0.46	−0.47	−0.06
H$^{1\prime}$	0.6	20.6	35.2	−0.57	−0.56	0.88	−0.08
			trans-equatorial [Cu(acac)$_2$Im$_{n=2}$]: DFT				
H^4	24.3	44.6	−11.2	0.09	−0.14	6.55	2.16
H^2	31.3	55.3	−41.2	6.52	−0.44	−0.31	1.92
H^5	16.1	74.9	−4.8	0.51	0.47	2.43	1.14
H^1	32.8	21.1	−34.2	3.15	1.10	1.25	1.83
H$^{4\prime}$	29.1	45.2	−13.2	0.10	−0.14	6.55	2.17
H$^{2\prime}$	33.6	57.0	−43.0	6.50	−0.44	−0.31	1.92
H$^{5\prime}$	18.9	75.1	−5.4	0.51	0.46	2.43	1.13
H$^{1\prime}$	38.9	22.9	−40.1	3.14	1.09	1.24	1.82

[a]For comparison, the DFT calculated ^{1}H hyperfine tensors for the geometry optimized adducts are also listed. Euler rotation of hyperfine tensor **A** to **g** tensor is given as a set of three Euler angles based on the *zyz′* convention. Euler angles are in degrees and their uncertainties are listed in footnotes a and b. [b]±10°: hyperfine tensor principal values are in MHz with uncertainty. [c]±0.4 MHz: for the bis-adducts, the protons from one Im unit are labeled H$^{1-5}$, and for the second Im unit, they are labeled H$^{1\prime-5\prime}$ (vide infra Figure 9).

slightly from axial symmetry with the largest principal axes approximately directed to the copper ion. According to the DFT geometry optimized structures, the ^{14}N hyperfine tensor calculated for the imino N^3 nitrogen in the *trans*-equatorial adduct most closely matched the experimental values (Table 4).

To corroborate the Q-band ENDOR experiments, additional angular selective X-band Davies ENDOR measurements were also performed (Figure 6b). As expected at this frequency, the spectra contain overlapping signals from both ^{1}H and ^{14}N nuclei in the region between 10−25 MHz. The broad line width of the ^{14}N signals prevented the accurate determination of $^{N}\boldsymbol{A}$ and $^{N}\boldsymbol{Q}$. Hyperfine selective Davies ENDOR measurements were also performed to suppress the ^{1}H signals without reducing or distorting the ^{14}N signals.[41] While proton suppression was successful, the ^{14}N signal remained broad and poorly resolved, as commonly observed for strongly coupled nitrogens in several copper proteins.[42,43] Nevertheless, an excellent fit to the experimental X-band Davies ENDOR was achieved using the ^{1}H and ^{14}N hyperfine tensors extracted from the Q-band spectra. The deconvoluted simulation of the Davies ENDOR is shown in the Supporting Information (Figure S4). The low anisotropy in the nitrogen hyperfine coupling is characteristic of Im coordination[36,44] and is typical of σ dominant bonding as expected for Cu(II)−Im coordination[45] (unlike for example *cis*- or *trans*-coordination of Cu−N2O2 as in Cu(II)-Salen complexes[46]). Combined, these observations are consistent with equatorial coordination of Im to [Cu(acac)$_2$].

The X-band HYSCORE spectrum of the [Cu(acac)$_2$Im$_2$] adduct complex (Figure 7) is characterized by cross peaks in both the (+,+) and (−,+) quadrants, arising from transitions associated with the remote amine ^{14}N nucleus of the imidazole ring (N^1). At X-band, the hyperfine coupling term for this specific ^{14}N interaction is approximately twice the nuclear Zeeman term, leading to the so-called cancellation condition such that the two terms cancel out in one of the two M_S spin manifolds. The nuclear frequencies of this particular M_S manifold corresponds to the nuclear quadrupolar resonance

DOI: 10.1021/acs.inorgchem.7b01874
Inorg. Chem. 2017, 56, 11862−11875

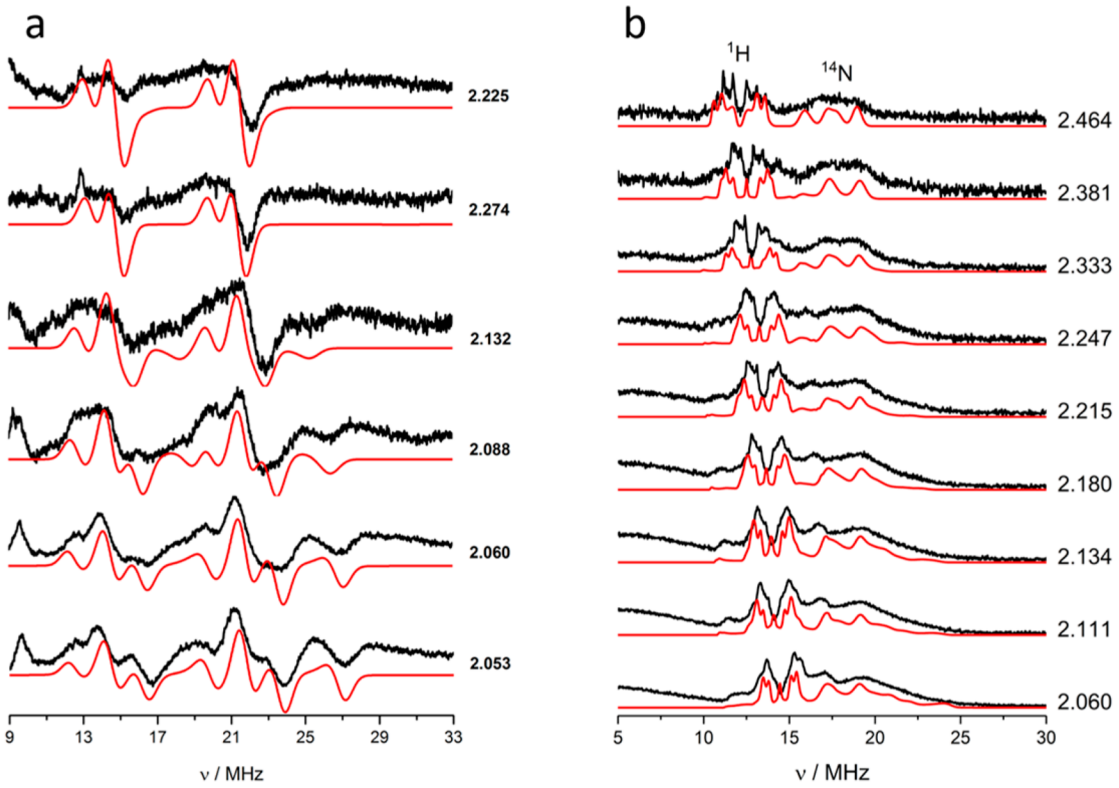

Figure 6. (a) Q-band CW ^{14}N ENDOR spectra and (b) X-band Davies ^{1}H and ^{14}N ENDOR spectra of the $[Cu(acac)_2Im_2]$ adduct dissolved in dry $CDCl_3$:DMF-d_7 (1:1). The spectra were measured at 10 K and recorded at the *g*-values indicated beside each spectrum. The corresponding simulations are shown in red.

(NQR) frequencies ν_-, ν_+, and ν_0, which appear in the ESEEM spectra at 0.7 MHz (ν_+) and 1.4 MHz ($\nu_- \approx \nu_0$). A feature appearing at about 4 MHz in the ESEEM spectrum is due to the nuclear double-quantum transition frequency, ν_{DQ} of the other M_S manifold.[47−49] The HYSCORE spectrum recorded at the maximum echo intensity (Figure 7a) is dominated by elongated cross peaks appearing at (±0.65, +4), (±4, +0.65), (±1.4, +4), and (±4, +1.4) MHz, which correspond to (ν_+,ν_{DQ}) and (ν_- (ν_0), ν_{DQ}) frequencies of the remote Im nitrogen nucleus, consistent with the ESEEM results. As reported by Mims and Peisach,[47] these frequencies correspond to a Fermi contact interaction term, a_{iso}, of 1.5−2.0 MHz, a nuclear quadrupole coupling $e^2qQ/h \approx 1.4$ MHz, and an asymmetry parameter, η, of 0.9−1. In addition to these signals, two cross peaks at about (2.2, 3.9) and (3.9, 2.2) MHz are present in the (+,+) quadrant, associated with the combination frequencies due to the presence of at least two remote nitrogen nuclei coupled to the same electron spin.[50] The HYSCORE spectra were thus simulated considering a three-spin system ($S = {}^1/_2$, $I_a = 1$, and $I_b = 1$) with two equivalent nitrogen nuclei with spin Hamiltonian parameters typical for remote ^{14}N nuclei of Im, as listed in Table 6.3. The simulations are displayed in red in Figure 7 and provide a convincing fit at both magnetic field settings. HYSCORE experiments thus indicate the presence of magnetically equivalent remote N^1 nitrogen atoms of Cu coordinated Im rings.

EPR Spectra of $[Cu(acac)_2]$ with Imidazole Derivatives (Im-2−4). We were also interested to explore whether the formation of the $[Cu(acac)_2Im_2]$ bis-adduct was limited to Im only. Hence, a number of other Im derivatives, including 2-methyl-imidazole (Im-**2**), 4(5)-methyl-imidazole (Im-**3**), and benzimidazole (Im-**4**), were also investigated (see Scheme 1). The EPR spectra of $[Cu(acac)_2]$ dissolved in $CHCl_3$:DMF containing increasing ratios of Im-**2**, Im-**3**, or Im-**4** are given in the Supporting Information (Figures S5−7). The corresponding EPR spectra recorded at a Cu:Im ratio of 1:50 are shown in Figure 8. At Cu:Im-**2**−**4** ratios of 1:10, only the monoaxial $[Cu(acac)_2$(Im-**2**−**4**)$]$ adducts were formed (Supporting Information, Figure S8), as revealed by the small changes in the *g* and ^{Cu}A values (Table 1). Moreover, at higher concentrations (Cu:Im-**2**−**4** ratios of 1:50), no further changes were detected in the EPR spectra for Im-**2** and Im-**4** (Figures 8c and b, respectively). By comparison, in the case of Im-**3**, the characteristic superhyperfine pattern observed in the EPR spectra of $[Cu(acac)_2Im_2]$ (Figures 1c and 8a) was also observed, indicating the formation of a $[Cu(acac)_2(Im\text{-}3)_2]$ bis-adduct (Figure 8d).

The absence of any bis-adducts for Im-**2** and Im-**4** must be attributed to steric effects because the basicity for all of the Im-derivatives is relatively large. Im-**4** is clearly too bulky to form the *trans*-equatorial conformation, whereas the presence of a methyl group in position 2 of Im-**2** also prevents formation of the *trans*-equatorial coordination mode. In contrast, in the case of Im-**3**, tautomerization will effectively result in the methyl group occurring at position 5 (see Scheme 1), therefore pointing away from the ligand methyl groups of the acetylacetonate units and thus enabling the formation of the *trans*-equatorial structure.

Coordination Mode of $[Cu(acac)_2Im_2]$. Over the years, numerous Cu(II) complexes have been studied as model systems to explore the structure, coordination, and binding in Cu(II) proteins. Invariably, studies of imidazole, substituted imidazoles, and histidine interactions with Cu(II) ions or complexes have been undertaken using EPR, ENDOR, and

DOI: 10.1021/acs.inorgchem.7b01874
Inorg. Chem. 2017, 56, 11862−11875

Table 4. Experimental and DFT Calculated ^{14}N Hyperfine and Nuclear Quadrupole Values of the $[Cu(acac)_2Im_2]$ Bis-Adduct[a]

label	α	β	γ	A_x	A_y	A_z	a_{iso}	$\lvert e^2qQ/h\rvert$	η	α'	β'	γ'
					$[Cu(acac)_2Im_{n=2}]$: experimental							
imino $N^{3,3'}$ (ENDOR)	0 ± 10	0 ± 10	−90 ± 5	34.8 ± 0.4	43.5 ± 0.4	34.0 ± 0.4	37.4 ± 0.4	2.2 ± 0.1	0.2 ± 0.1	0 ± 10	0 ± 10	−90 ± 5
amine $N^{1,1'}$ (HYSCORE)	85 ± 5	80 ± 10	0	1.5 ± 0.2	1.4 ± 0.2	2.5 ± 0.2	1.8 ± 0.2	1.4 ± 0.1	0.9 ± 0.1	15 ± 15	−10 ± 15	0 ± 15
					cis-mixed plane $[Cu(acac)_2Im_2]$							
imino N^3	−0.7	88.8	7.3	−0.50	−1.42	−1.42	−1.11	3.4	0.2	−14.1	88.2	2.4
amine N^1	−7.2	79.8	−1.7	0.02	−0.16	−0.16	−0.10	2.9	0.1	−21.4	42.1	18.3
imino $N^{3'}$	−1.3	86.9	−1.8	29.25	35.95	28.55	31.25	2.7	0.4	−0.1	87.1	−0.5
amine $N^{1'}$	0	87.5	1.4	1.46	1.96	1.60	1.67	2.8	0.05	1.6	87.8	−35.1
					trans-axial $[Cu(acac)_2Im_2]$							
imino N^3	5.7	1.1	108.6	−1.62	−1.64	−0.74	−1.33	3.4	0.2	24.4	11.6	23.7
amine N^1	7.4	14.0	39.2	−0.17	−0.17	0.01	−0.11	2.9	0.1	5.2	63.3	44.5
imino $N^{3'}$	6.6	1.4	−40.1	−1.61	−1.63	−0.73	−1.32	3.4	0.2	−35.6	14.5	57.1
amine $N^{1'}$	−12.2	15.0	36.9	−0.16	−0.17	0.01	−0.11	2.9	0.1	−9.1	64.9	27.2
					trans-equatorial $[Cu(acac)_2Im_2]$							
imino N^3	−6.9	8.3	−85.0	37.45	45.31	36.40	39.72	2.5	0.5	−9.3	9.2	−82.5
amine N^1	−19.0	9.3	−72.40	2.25	2.83	2.40	2.49	2.9	0.05	11.0	57.2	−8.2
imino $N^{3'}$	−6.1	10.5	−85.8	37.42	45.27	36.37	39.69	2.5	0.5	−8.0	11.6	−83.9
amine $N^{1'}$	−15.5	11.7	−76.1	2.24	2.83	2.40	2.49	2.9	0.05	13.5	58.5	−9.5

[a]The experimental values were obtained by ENDOR (for the imino $N^{3,3'}$) and HYSCORE (for the amine $N^{1,1'}$). Hyperfine tensor principal values and nuclear quadrupole coupling are given in units of MHz; Euler angles, referred to the *g*-frame, are given in degrees.

DOI: 10.1021/acs.inorgchem.7b01874
Inorg. Chem. 2017, 56, 11862−11875

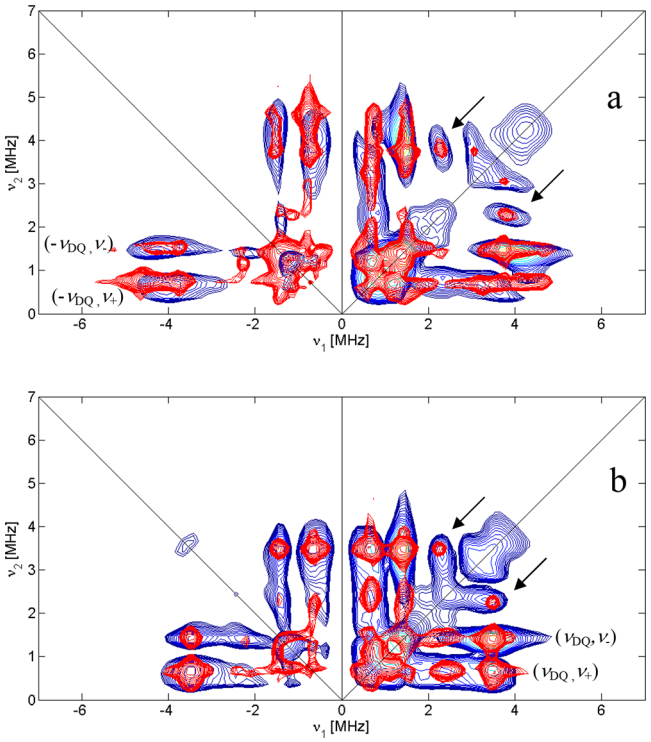

Figure 7. 2D HYSCORE spectra of $[Cu(acac)_2Im_2]$ recorded at B_0 = 338.6 mT and τ = 176 ns (a) and B_0 = 283.2 mT and τ = 144 ns (b). Both spectra were recorded at 10 K. The assignments of the cross-peaks are shown on the spectrum. The arrows indicate the combination peaks.

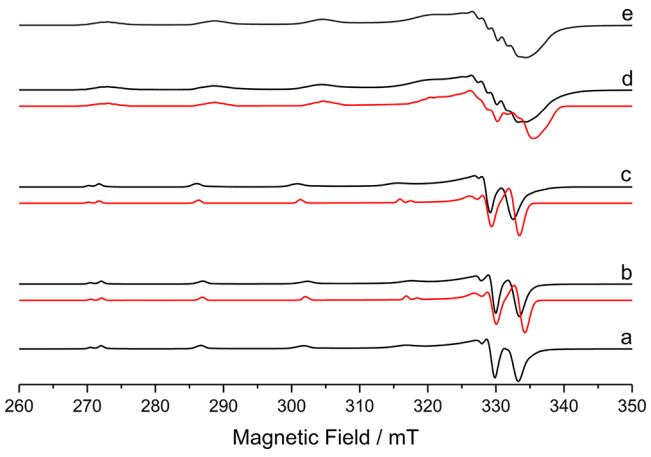

Figure 8. Experimental (black) and simulated (red) CW X-band EPR spectra of (a) $[Cu(acac)_2Im]$, (b) $[Cu(acac)_2(Im\text{-}\mathbf{4})]$, (c) $[Cu(acac)_2(Im\text{-}\mathbf{2})]$, (d) $[Cu(acac)_2(Im\text{-}\mathbf{3})_2]$, and (e) $[Cu(acac)_2Im_2]$. The spectra were recorded at 140 K in a $CHCl_3$:DMF (1:1) solvent with a Cu:Im-**1**−**4** ratio of 1:50 in all cases. The simulated spectra for a and e are shown in Figure 1. The simulation parameters are listed in Table 1.

ESEEM,[51−53] largely because imidazole is an important component (as the side chain histidine and a constituent of purine bases) of many proteins. Although the imino nitrogen N^3 is the common binding site for metal ions (Scheme 1), in deprotonated Im, both nitrogens are sufficiently basic enough to facilitate binding. Therefore, the study of Im coordination is extremely important for the evaluation of the binding between metal ions and the imidazole residues of proteins.[1,4] In many cases, the combined use of EPR and ENDOR or ESEEM was employed to determine the complete conformation of the coordinated substrates by analysis of the ^1H and ^{14}N hyperfine and (^{14}N) quadrupole parameters.[28,31,36,37,44,45,47,48,51,54] However, a growing number of mixed chelate Cu(II) complexes containing the acetylacetonate ligand and a bidentate nitrogen-based N−N ligand (i.e., [Cu(acac)(N−N)]) have received considerable interest recently owing to their cytotoxicity and DNA binding capabilities,[4,55] but the interaction of these mixed and simple chelate complexes with imidazole has not been investigated to date.

The current study considered a number of possible conformations for the $[Cu(acac)_2Im_2]$ bis-adducts in solution. Through a combined computational and experimental EPR approach, an accurate assignment to one particular coordination mode (i.e., *trans*-equatorial $[Cu(acac)_2Im_2]$) was established. Initially at low Im concentrations, the monoaxial $[Cu(acac)_2Im]$ adduct is formed, as confirmed by the small shift in g and ^{Cu}A values relative to the unbound $[Cu(acac)_2]$ complex (Table 1). At higher Im concentrations, a bis-adduct was formed as revealed by the ^{14}N superhyperfine pattern on the $m_I = +^3/_2$ $^{63,64}Cu$ hyperfine component. Owing to the strong basicity of the Im substrate, the in-plane bis-(acetylacetonato) ligands must rearrange to facilitate the in-plane equatorial coordination of the two Im units. The resulting tetragonally distorted octahedral complex contains a Cu−N2O2 plane with the two coordinating nitrogens coming from the N^3 Im substrate. The g_x component of the **g** tensor is positioned along this equatorial N−Cu−N direction with the g_y component lying almost along the equatorial O−Cu−O direction and with g_z almost along the axial O−Cu−O direction (Figure 9). Orientation selective ^1H ENDOR revealed the hyperfine couplings to three sets of protons on the Im ring. The two protons adjacent to the imino N^3 nitrogen (H^2 and H^4) gave similar hyperfine tensors according to the DFT calculations, which were indistinguishable in the experimental ENDOR spectra. The remaining two protons (labeled H^5 and H^1 in Scheme 1) produced sufficiently different hyperfine tensors so that all proton sets could be distinguished in the angular selective ^1H ENDOR simulations.

Angular selective ^{14}N ENDOR spectra were also recorded at X-band (Davies ENDOR) and Q-band (CW ENDOR) frequencies, yielding information on the hyperfine coupling and nuclear quadrupole coupling to the coordinating N^3 nitrogen (Table 4). The ^{14}N hyperfine tensor of the imino N^3 nitrogen was found to be nearly axially symmetric with the largest principal axis, ^NA_y, oriented almost directly along the Cu−N bond direction and the g_x-component (Figure 9). The experimental and theoretical ^NA values for the *trans*-equatorial $[Cu(acac)_2Im_2]$ structure were in excellent agreement with each other ([34.8, 43.5, 34.0] versus [37.4, 45.3, 36.4] MHz, respectively). The ^NA values for the *cis*-mixed plane and *trans*-axial structures were by comparison considerably smaller ([29.2, 35.9, 28.5] and [−1.62, −1.64, −0.74] MHz respectively; Table 4). The experimental e^2qQ/h and η values were also typical for strongly coordinating nitrogens in Cu−N2O2-type complexes. The experimental ^NA values for the remote N^1 Im nitrogen, as determined by HYSCORE, were smaller compared to the theoretical values (Table 4) because DFT often overestimates these parameters for remote nitrogens. Nevertheless, the observed values were in the region expected for equatorially bound Im and were certainly larger than those predicted for the *cis*-mixed plane and *trans*-axial structures. Taken together, it is clear that the ^{14}N ENDOR and

DOI: 10.1021/acs.inorgchem.7b01874
Inorg. Chem. 2017, 56, 11862−11875

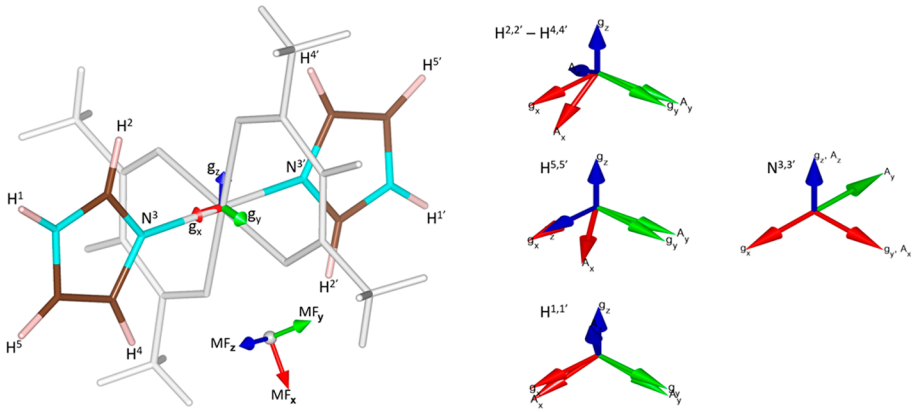

Figure 9. Geometry optimized DFT structure for the *trans*-equatorial $[Cu(acac)_2Im_2]$ adduct, showing the relative orientation of the ^1H and ^{14}N hyperfine tensors with respect to the *g*-frame.

HYSCORE analysis is entirely consistent with the formation of the *trans*-equatorial $[Cu(acac)_2Im_2]$ adduct.

CONCLUSION

An experimental (EPR, ENDOR, and HYSCORE) and computational study of imidazole interactions with a simple $[Cu(acac)_2]$ complex was undertaken. A growing number of cytoxic Cu(II)-based complexes contain the acetylacetonate ligand; therefore, a better understanding of how such complexes interact with imidazole, representing the side chain of the amino acid histidine, for example, is experimentally important. At a relatively low ratio of Cu to Im, a $[Cu(acac)_2Im_{n=1}]$ monoadduct is formed. The Im was found to coordinate in the axial position, as confirmed by the small shift in the g_3 value (Δg_z = 0.022) and the concomitant decrease in the $^{Cu}A_3$ value (ΔA_z = 48 MHz) relative to the unbound $[Cu(acac)_2]$ complex. At higher ratios of Cu to Im, a $[Cu(acac)_2Im_2]$ bis-adduct is formed, as revealed by the superhyperfine pattern detected in the CW EPR spectra, which can be interpreted only based on two strongly coordinating and largely equivalent nitrogens. Different structural isomers of this bis-adduct are possible, and detailed ^1H and ^{14}N hyperfine analysis reveals that the *trans*-equatorial conformer is formed. Three individual sets of ^1H tensors were detected in the ENDOR spectra and assigned to the H^2/H^4, H^5, and H^1 protons of Im. These values were consistent with either a *cis*-mixed plane or *trans*-equatorial structure for $[Cu(acac)_2Im_2]$. However, angular selective ^{14}N ENDOR (both CW and pulsed) provided more detailed insights into the hyperfine and quadrupole values for the coordinating imino N^3 nitrogen; these parameters were in excellent agreement with the geometry optimized structure for the *trans*-equatorial $[Cu(acac)_2Im_2]$ structure only. Equally, the hyperfine and quadrupole values for the remote amine ^{14}N were determined by simulation of the X-band HYSCORE spectra, and a reasonably good agreement was achieved between theory and experiment. The ability of the coordinating ligand in the Cu-based complexes to flip between *cis*- and *trans*-conformations (from unbound to Im-bound adducts) must therefore be considered when designing novel cytotoxic Cu(II)-based complexes for target interactions with proteins bearing imidazole residues.

ASSOCIATED CONTENT

Supporting Information

The Supporting Information is available free of charge on the ACS Publications website at DOI: 10.1021/acs.inorgchem.7b01874.

CW EPR spectra (140 K) of $[Cu(acac)_2]$ with increasing Im ratios; EPR spectra (298 K) of $[Cu(acac)_2]$ + Im at 1:10 ratio; Q-band ^1H ENDOR spectra (10 K) of $[Cu(acac)_2Im_{n=2}]$ in protic and deuterated Im; deconvoluted simulation of X-band Davies ENDOR for $[Cu(acac)_2Im_{n=2}]$; CW EPR spectra of $[Cu(acac)_2]$ with increasing concentrations of Im-**2**–**4**; experimental and simulated EPR spectra of $[Cu(acac)_2]$ with a Cu:Im-**2**–**4** ratio of 1:10 (PDF)

AUTHOR INFORMATION

Corresponding Authors

*E-mail: RichardsE10@cardiff.ac.uk.
*E-mail: FolliA@cardiff.ac.uk.
*E-mail: MurphyDM@cardiff.ac.uk.

ORCID

Andrea Folli: 0000-0001-8913-6606
Mario Chiesa: 0000-0001-8128-8031
Damien M. Murphy: 0000-0002-5941-4879

Notes

The authors declare no competing financial interest.

ACKNOWLEDGMENTS

We acknowledge the EPSRC (Grants EP/K017322/1 and EP/P019951/1) for financial support.

REFERENCES

(1) Orvig, C.; Abrams, M. J. Medicinal Inorganic Chemistry: Introduction. *Chem. Rev.* **1999**, *99*, 2201–2203.
(2) Ronconi, L.; Sadler, P. J. Using coordination chemistry to design new medicines. *Coord. Chem. Rev.* **2007**, *251*, 1633–1648.
(3) Holm, R. H.; Kennepohl, P.; Solomon, E. I. Structural and Functional Aspects of Metal Sites in Biology. *Chem. Rev.* **1996**, *96*, 2239–2314.
(4) Santini, C.; Pellei, M.; Gandin, V.; Porchia, M.; Marzano, C. Advances in copper complexes as anticancer agents. *Chem. Rev.* **2014**, *114*, 815–862.
(5) Liu, H.-K.; Sadler, P. J. Metal complexes as DNA intercalators. *Acc. Chem. Res.* **2011**, *44*, 349–359.

DOI: 10.1021/acs.inorgchem.7b01874
Inorg. Chem. 2017, 56, 11862–11875

(6) Kostova, I. Titanium and vanadium complexes as anticancer agents. *Anti-Cancer Agents Med. Chem.* **2009**, *9*, 827−842.
(7) (a) Hoffman, B. M. Electron-nuclear double resonance spectroscopy (and electron spin-echo envelope modulation spectroscopy) in bioinorganic chemistry. *Proc. Natl. Acad. Sci. U. S. A.* **2003**, *100*, 3575−3578. (b) Solomon, E. I.; Heppner, D. E.; Johnston, E. M.; Ginsbach, J. W.; Cirera, J.; Qayyum, M.; Kieber-Emmons, M. T.; Kjaergaard, C. H.; Hadt, R. G.; Tian, L. Copper Active Sites in Biology. *Chem. Rev.* **2014**, *114*, 3659−3853. (c) Solomon, E. I.; Szilagyi, R. K.; DeBeer George, S.; Basumallick, L. Electronic Structures of Metal Sites in Proteins and Models: Contributions to Function in Blue Copper Proteins. *Chem. Rev.* **2004**, *104*, 419−458.
(8) Sánchez-Guadarrama, O.; López-Sandoval, H.; Sánchez-Bartéz, F.; Gracia-Mora, I.; Höpfl, H.; Barba-Behrens, N. Cytotoxic activity, X-ray crystal structures and spectroscopic characterization of cobalt(II), copper(II) and zinc(II) coordination compounds with 2-substituted benzimidazoles. *J. Inorg. Biochem.* **2009**, *103*, 1204−1213.
(9) Webb, M. I.; Walsby, C. J. Albumin binding and ligand-exchange processes of the Ru(III) anticancer agent NAMI-A and its bis-DMSO analogue determined by ENDOR spectroscopy. *Dalton Trans.* **2015**, *44*, 17482−17493.
(10) Davies, E. R. A new pulsed endor technique. *Phys. Lett. A* **1974**, *47*, 1−2.
(11) Höfer, P.; Grupp, A.; Nebenführ, H.; Mehring, M. Hyperfine Sublevel Correlation (HYSCORE) Spectroscopy: a 2D ESR Investigation of the Squaric Acid Radical. *Chem. Phys. Lett.* **1986**, *132*, 279−282.
(12) Stoll, S.; Schweiger, A. EasySpin, a comprehensive software package for spectral simulation and analysis in EPR. *J. Magn. Reson.* **2006**, *178*, 42−55.
(13) Atherton, N. *Principles of Electron Spin Resonance*; Ellis Horwood Limited, 1993.
(14) Freed, J. H.; Fraenkel, G. K. Theory of linewidths in electron spin resonance spectra. *J. Chem. Phys.* **1963**, *39*, 326−348.
(15) Zhao, Y.; Truhlar, D. G. The M06 suite of density functionals for main group thermochemistry, thermochemical kinetics, noncovalent interactions, excited states, and transition elements: two new functionals and systematic testing of four M06-class functionals and 12 other functionals. *Theor. Chem. Acc.* **2008**, *120*, 215−41.
(16) Ditchfield, R.; Hehre, W. J.; Pople, J. A. Self-consistent molecular-orbital methods. IX. Extended Gaussian-type basis for molecular-orbital studies of organic molecules. *J. Chem. Phys.* **1971**, *54*, 724−8.
(17) Hariharan, P. C.; Pople, J. A. The influence of polarization functions on molecular orbital hydrogenation energies. *Theor. Chem. Acc.* **1973**, *28*, 213−222.
(18) Clark, T.; Chandrasekhar, J.; Spitznagel, G. W.; Schleyer, P.v.R. Efficient diffuse function-augmented basis sets for anion calculations. III. The 3-21+G basis set for first-row elements, Li−F. *J. Comput. Chem.* **1983**, *4*, 294−301.
(19) Dolg, M.; Wedig, U.; Stoll, H.; Preuss, H. Energy-adjusted ab initio pseudopotentials for the first row transition elements. *J. Chem. Phys.* **1987**, *86*, 866−872.
(20) Frisch, M. J.; et al. *Gaussian 09*, revision C.01; Gaussian, Inc.: Wallingford, CT, 2010.
(21) Neese, F. The ORCA program system. *Wiley Interdiscip. Rev.: Comput. Mol. Sci.* **2012**, *2*, 73.
(22) Adamo, C.; Barone, V. Toward reliable density functional methods without adjustable parameters: The PBE0 model. *J. Chem. Phys.* **1999**, *110*, 6158−6169.
(23) Barone, V. *Recent Advances in Density Functional Methods*, Part I; Chong, D. P., Ed.; World Scientific Publ. Co.: Singapore, 1996.
(24) The ORCA basis set CoreProp was used. This basis is based on theTurboMole DZ basis developed by Ahlrichs and coworkers and obtained from the basis set library under ftp.chemie.uni-karlsruhe.de/pub/basen.
(25) Neese, F. Efficient and Accurate Approximations to the Molecular Spin-Orbit Coupling Operator and Their Use in Molecular g-Tensor Calculations. *J. Chem. Phys.* **2005**, *122*, 34107.
(26) Sharples, K. M.; Carter, E.; Hughes, C. W.; Harris, K. D. M.; Platts, J. A.; Murphy, D. M. An ENDOR and DFT analysis of hindered methyl group rotations in frozen solutions of bis(acetylacetonato)-copper(II). *Phys. Chem. Chem. Phys.* **2013**, *15*, 15214−15222.
(27) Carter, E.; Sharples, K. M.; Platts, J. A.; Murphy, D. M. Structure determination of bound nitrogen-based adducts with copper(II) acetylacetonato; an EPR, ENDOR and DFT study. *Phys. Chem. Chem. Phys.* **2015**, *17*, 11445−11454.
(28) Bonomo, R. P.; Riggi, F.; Di Bilio, A. J. EPR reinvestigation of the Copper(II)-imidazole system. *Inorg. Chem.* **1988**, *27*, 2510−2512.
(29) Attanasio, D.; Collamati, I.; Ercolani, C. Ligand arrangement and tetragonal distortion in CuO_4N_2 chromophores studied by electronic and electron spin resonance spectroscopy. *J. Chem. Soc., Dalton Trans.* **1974**, 1319−1324.
(30) Wayland, B. B.; Kapur, V. K. Electron paramagnetic resonance and electronic spectral evidence for isomers resulting from basal and axial ligation of bis(hexafluoroacetylacetonato)copper(II) by triphenylphosphine. *Inorg. Chem.* **1974**, *13*, 2517−2520.
(31) Siddiqui, S.; Shepherd, R. E. Electron spin resonance studies of copper(II) polyamine and imidazole complexes. *Inorg. Chem.* **1986**, *25*, 3869−3876.
(32) Bersuker, I. B. Modern Aspects of the Jahn−Teller Effect Theory and Applications To Molecular Problems. *Chem. Rev.* **2001**, *101*, 1067−1114.
(33) Veidis, M. V.; Schreiber, G. H.; Gough, T. E.; Palenik, G. J. Jahn-Teller distortions in octahedral copper(II) complexes. *J. Am. Chem. Soc.* **1969**, *91*, 1859−1860.
(34) Attanasio, D.; Collamati, I.; Ercolani, C.; Rotilio, G. Complexing properties of α-nitroketones. Part III. A stereochemical investigation of some new copper(II)α-nitroketonate complexes and their base adducts with O- and N-donors. *J. Chem. Soc., Dalton Trans.* **1973**, 2242−2247.
(35) (a) Iwaizumi, M.; Kudo, T.; Kita, S. Correlation between the hyperfine coupling constants of donor nitrogens and the structures of the first coordination sphere in copper complexes as studied by nitrogen-14 ENDOR spectroscopy. *Inorg. Chem.* **1986**, *25*, 1546−1550. (b) Miyamoto, R.; Ohba, Y.; Iwaizumi, M. Angle selected ^{14}N-ENDOR of copper(II) complexes with distorted N_2S_2 and N_2O_2 coordination structures. *Inorg. Chem.* **1992**, *31*, 3138−3149.
(36) Van Camp, H. L.; Sands, R. H.; Fee, J. A. Electron-nuclear double resonance on copper(II) tetraimidazole. *J. Chem. Phys.* **1981**, *75*, 2098−2107.
(37) Andersson, M.; Hedin, J.; Johansson, P.; Nordstrom, J.; Nyden, M. Coordination of Imidazoles by Cu(II) and Zn(II) as Studied by NMR Relaxometry, EPR, far-FTIR Vibrational Spectroscopy and Ab Initio Calculations: Effect of Methyl Substitution. *J. Phys. Chem. A* **2010**, *114*, 13146−13153.
(38) (a) Rahaman, S. H.; Chowdhury, H.; Bose, D.; Mostafa, G.; Fun, H.-K.; Ghosh, B. K. 1D polymeric chain of copper(II) containing imidazolate and perchlorate bridging: supramolecular synthon involving N-H···O hydrogen bonding. *Inorg. Chem. Commun.* **2005**, *8*, 1041−1044. (b) Higa, T.; Moriya, M.; Shimazaki, Y.; Yajima, T.; Tani, F.; Karasawa, S.; Nakano, M.; Naruta, Y.; Yamauchi, O. Synthesis and characterization of imidazolate-bridged polynuclear copper complexes. *Inorg. Chim. Acta* **2007**, *360*, 3304−3313. (c) Chaudhuri, P.; Karpenstein, I.; Winter, M.; Lengen, M.; Butzlaff, C.; Bill, E.; Trautwein, A. X.; Floerke, U.; Haupt, H. J. An imidazolate-bridged tetranuclear copper(II) complex: synthesis, magnetic and EPR studies, and crystal structure of [L4Cu4(Im)4](ClO4)4.2H2O (L = 1,4,7-triazacyclononane, Im = imidazolate anion). *Inorg. Chem.* **1993**, *32*, 888−894. (d) Alves, W. A.; Cerchiaro, G.; Paduan-Filho, A.; Tomazela, D. M.; Eberlin, M. N.; Da Costa Ferreira, A. M. Infinite zig-zag and cyclic-tetranuclear isomeric imidazolate-bridged polynuclear copper(II) complexes: Magnetic properties, catalytic activity and electrospray mass and tandem mass spectrometry characterization. *Inorg. Chim. Acta* **2005**, *358*, 3581−3591. (e) Masciocchi, N.; Ardizzoia, G. A.; LaMonica, G.; Maspero, A.; Galli, S.; Sironi, A. Metal Imidazolato Complexes: Synthesis, Characterization, and X-ray

DOI: 10.1021/acs.inorgchem.7b01874
Inorg. Chem. 2017, 56, 11862−11875

Powder Diffraction Studies of Group 10 Coordination Polymers. *Inorg. Chem.* **2001**, *40*, 6983−6989.
(39) Strothkamp, K. G.; Lippard, S. J. Chemistry of the imidazolate-bridged bimetallic center in the copper-zinc superoxide dismutase and its model compounds. *Acc. Chem. Res.* **1982**, *15*, 318−326.
(40) (a) Koch, C. A.; Reed, C. A.; Brewer, G. A.; Rath, N. P.; Scheidt, W. R.; Gupta, G.; Lang, G. Ferromagnetic Coupling Via Imidazolate in an Iron (III) Porphyrin Dicopper (II) System. *J. Am. Chem. Soc.* **1989**, *111*, 7645−7648. (b) Song, Y. F.; Massera, C.; Quesada, M.; Koval, I. A.; Gamez, P.; Manotti Lanfredi, A. M.; Reedijk, J. A New Trinuclear Linear Copper(II) Complex: Unusual Crystal Structure with Semi-Coordinated Thiophene Moieties and Weak Antiferromagnetic Coupling Through the Bridging Imidazolate Rings. *Eur. J. Inorg. Chem.* **2004**, *2004*, 4566−4571. (c) Kolks, G.; Lippard, S. J.; Waszczak, J. V.; Lilienthal, H. R. Magnetic exchange in imidazolate-bridged copper(II) complexes. *J. Am. Chem. Soc.* **1982**, *104*, 717−725.
(41) (a) Fan, C.; Doan, P. E.; Davoust, C. E.; Hoffman, B. M. Quantitative studies of Davies pulsed ENDOR. *J. Magn. Reson.* **1992**, *98*, 62−72. (b) Doan, P. E.; Fan, C.; Davoust, C. E.; Hoffman, B. M. A simple method for hyperfine-selective heteronuclear pulsed ENDOR via proton suppression. *J. Magn. Reson.* **1991**, *95*, 196−200.
(42) Van Camp, H. L.; Wei, Y. H.; Scholes, C. P.; King, T. E. Electron nuclear double resonance of cytochrome oxidase: nitrogen and proton ENDOR from the 'copper' EPR signal. *Biochim. Biophys. Acta, Protein Struct.* **1978**, *537*, 238−246.
(43) Rist, G. H.; Hyde, J. S.; Vänngård, T. Electron-Nuclear Double Resonance of a Protein That Contains Copper: Evidence for Nitrogen Coordination to Cu(II) in Stellacyanin. *Proc. Natl. Acad. Sci. U. S. A.* **1970**, *67*, 79−86.
(44) Yokoi, H. ^{14}N-ENDOR evidence for imidazole coordination in copper proteins. *Biochem. Biophys. Res. Commun.* **1982**, *108*, 1278−1284.
(45) Sundberg, R. J.; Martin, R. B. Interactions of histidine and other imidazole derivatives with transition metal ions in chemical and biological systems. *Chem. Rev.* **1974**, *74*, 471−517.
(46) (a) Kita, S.; Hashimoto, M.; Iwaizumi, M. ENDOR Studies of [N,N′-Ethylenebis(salicylideniminato)]copper(II) in [N,N′-Ethylenebis(salicylideniminato)] nickel(II) Single Crystals. *Inorg. Chem.* **1979**, *18*, 3432−3438. (b) Murphy, D. M.; Caretti, I.; Carter, E.; Fallis, I. A.; Gobel, M. C.; Landon, J.; Van Doorslaer, S.; Willock, D. J. Visualizing Diastereomeric Interactions of Chiral Amine Chiral Copper Salen Adducts by EPR Spectroscopy and DFT. *Inorg. Chem.* **2011**, *50*, 6944−6955.
(47) Mims, W. B.; Peisach, J. The nuclear modulation effect in electron spin echoes for complexes of copper(2+) ion and imidazole with nitrogen-14 and nitrogen-15. *J. Chem. Phys.* **1978**, *69*, 4921−4930.
(48) Jiang, F.; McCracken, J.; Peisach, J. Nuclear quadrupole interactions in copper(II)-diethylenetriamine-substituted imidazole complexes and in copper(II) proteins. *J. Am. Chem. Soc.* **1990**, *112*, 9035−9044.
(49) Flanagan, H. L.; Singel, D. J. Analysis of nitrogen-14 ESEEM patterns of randomly oriented solids. *J. Chem. Phys.* **1987**, *87*, 5606−5616.
(50) McCracken, J.; Pember, S.; Benkovic, S. J.; Villafranca, J. J.; Miller, R. J.; Peisach, J. Electron spin-echo studies of the copper binding site in phenylalanine hydroxylase from Chromobacterium violaceum. *J. Am. Chem. Soc.* **1988**, *110*, 1069−1074.
(51) Jiang, F.; Karlin, K. D.; Peisach, J. An electron spin echo envelope modulation (ESEEM) study of electron-nuclear hyperfine and nuclear quadrupole interactions of d_{z^2} ground state copper(II) complexes with substituted imidazoles. *Inorg. Chem.* **1993**, *32*, 2576−2582.
(52) Manikandan, P.; Epel, B.; Goldfarb, D. Structure of copper(II)-histidine based complexes in frozen aquesous solutions as determined from high-field pulsed electron nuclear double resonance. *Inorg. Chem.* **2001**, *40*, 781−787.
(53) Scholl, H.-J.; Huttermann, J. ESR and ENDOR of Cu(II) complexes with nitrogen donors: probing parameters for prosthetic group modelling of superoxide dismutase. *J. Phys. Chem.* **1992**, *96*, 9684−9691.
(54) Ashby, C. I. H.; Cheng, C. P.; Brown, T. L. ^{14}N Nuclear quadrupole resonance spectra of coordinated imidazole. *J. Am. Chem. Soc.* **1978**, *100*, 6057−6063.
(55) (a) Chen, G.-J.; Qiao, X.; Qiao, P.-Q.; Xu, G.-J.; Xu, J.-Y.; Tian, J.-l.; Gu, W.; Liu, X.; Yan, S.-P. Synthesis, DNA binding, photo-induced DNA cleavage, cytotoxicity and apoptosis studies of copper(II) complexes. *J. Inorg. Biochem.* **2011**, *105*, 119−126. (b) Tovar-Tovar, A.; Ruiz-Ramırez, L.; Campero, A.; Romerosa, A.; Moreno-Esparza, R.; Rosales-Hoz, M. J. Structural and reactivity studies on 4,4′-dimethyl-2,2′-bipyridine acetylacetonate copper(II) nitrate (CASIOPEINA III-ia) with methionine, by UV−visible and EPR techniques. *J. Inorg. Biochem.* **2004**, *98*, 1045−1053. (c) Zhao, X.-F.; Ouyang, Y.; Liu, Y.-Z.; Su, S.; Tian, H.; Xie, C.-Z.; Xu, J.-Y. Two polypyridyl copper(II) complexes: synthesis, crystal structure and interaction with DNA and serum protein in vitro. *New J. Chem.* **2014**, *38*, 955−965.

DOI: 10.1021/acs.inorgchem.7b01874
Inorg. Chem. 2017, 56, 11862−11875